

56 2 Stabilizer Formalism

57 A well-developed framework used to efficiently characterize quantum error correction codes is the *stabilizer*
 58 *formalism*. It describes a code space as the simultaneous $+1$ eigenspace of a set of commuting Pauli operators,
 59 called *stabilizers*. Errors are detected by measuring these stabilizers: if an error anticommutes with a
 60 stabilizer, the corresponding measurement outcome flips, providing an error syndrome.

61 **Stabilizer code.** A *stabilizer code* on n qubits is specified by an abelian subgroup $\mathcal{S} \subseteq \mathcal{P}_n$ (the n -qubit
 62 Pauli group) that does not contain $-I$. The *codespace* \mathcal{C} is the joint $+1$ eigenspace of all elements of \mathcal{S} :

$$\mathcal{C} = \{ |\psi\rangle \in (\mathbb{C}^2)^{\otimes n} : S|\psi\rangle = |\psi\rangle \quad \forall S \in \mathcal{S} \}.$$

63 **Dimension.** If the code encodes k logical qubits into n physical qubits (an $[[n, k, d]]$ code), then with $n - k$
 64 independent stabilizer generators we have

$$\dim \mathcal{C} = \frac{2^n}{2^{n-k}} = 2^k.$$

65 **Logical basis inside the codespace.** Because $\dim \mathcal{C} = 2^k$, we may choose an orthonormal *logical basis*
 66 of \mathcal{C} ,

$$\mathcal{B}_L = \{ |x_L\rangle : x \in \{0, 1\}^k \},$$

67 such that each basis vector lies in the codespace (hence is stabilized):

$$S|x_L\rangle = |x_L\rangle \quad \forall S \in \mathcal{S}, \quad \forall x \in \{0, 1\}^k.$$

68 **Arbitrary logical state (spanning by the logical basis).** Any generic codespace vector $|\psi\rangle \in \mathcal{C}$ can
 69 be expressed *in the logical basis* as

$$|\psi\rangle \equiv |\psi_L\rangle = \sum_{x \in \{0, 1\}^k} \alpha_x |x_L\rangle, \quad \sum_x |\alpha_x|^2 = 1.$$

70 Thus the logical basis $\{|x_L\rangle\}$ spans the same subspace that was defined abstractly by the condition $S|\psi\rangle =$
 71 $|\psi\rangle$.

72 **Expansion in the physical (computational) basis.** Each logical basis vector is itself a vector in the
 73 n -qubit Hilbert space and typically expands as a superposition of computational basis states:

$$|x_L\rangle = \sum_{i=0}^{2^n-1} c_i^{(x)} |i\rangle,$$

74 with coefficients $\{c_i^{(x)}\}$ constrained by the stabilizer conditions $S|x_L\rangle = |x_L\rangle$ for all $S \in \mathcal{S}$. These constraints
 75 select which computational-basis components may appear and with what relative phases or amplitudes.

76 **Remark (stabilizers vs. logical operators).** Stabilizers act *trivially* on every codespace vector (eigen-
 77 value $+1$) and thus define \mathcal{C} . By contrast, *logical operators* act *nontrivially* within \mathcal{C} ; they lie in the normalizer
 78 $N(\mathcal{S})$ of \mathcal{S} in \mathcal{P}_n but not in \mathcal{S} itself.

79 There are $n - k$ independent stabilizer generators, which generate the full stabilizer group of size $|\mathcal{S}| =$
 80 2^{n-k} . These $n - k$ constraints reduce the full 2^n -dimensional Hilbert space to the 2^k -dimensional code space.
 81 In other words:

- 82 • n physical qubits provide a Hilbert space of dimension 2^n ,

- 83 • $n - k$ stabilizer constraints remove $n - k$ degrees of freedom,
 84 • leaving k logical qubits, i.e. a code space of dimension 2^k (same as logical state dimension).

85 Within this framework, many of the most important quantum error correction codes—including repetition
 86 codes, concatenated codes (e.g., Shor code), the color code of Hamming codes (e.g., Steane code), surface
 87 codes, and subsystem codes (e.g., Bacon-Shor code)—can be described in a unified and elegant way.

88 3 Homomorphic Logical Measurements (Notes on the Talk and 89 Paper [5, 7])

90 3.1 Surface code

91 Each stabilizer act on neighbor local qubits. The error threshold is low but the code distance cannot be well
 92 increased even with larger physical qubits number. The relation write $kd^2 = O(n)$ with n, k, d being the
 93 typical $[[n, k, d]]$ definition error code. Here we can see that if restricting on encoding rates $\frac{k}{n} \sim 1$, code
 94 distance d scales as $O(1)$. Noted that for linear code, $n \geq k + d - 1$

95 3.2 Quantum LDPC (Low-Density Parity-Check) code

96 Decoding time is large to cost computation delays, while fast decoding is an essential ingredient to fault-
 97 tolerant computation. Sparce stabilizers (low weight hamming weight) can improve the problem [12]. Quan-
 98 tum LDPC code provide nonlocal stabilizers, measurements. The code distance d can be increased faster not
 99 following $kd^2 = n$ (code rate: $\frac{k}{n}$). In addition, one motivation comes from when standard Shor and Steane
 100 style logical measurement cannnot be performed on large quantum LDPC code.

101 For typical surface code, code rate scales asymptotically to zero and with square root of code distance
 102 when enlarging code block. Improvement gives nonvanishing encoding rate for different surfaces (more non-
 103 trivial loops), but with code distance logarithmic in the blocklength. **Hypergraph product construction**
 104 improve this problem: First of all, we have

$$\text{Toric code} \subset \text{Hypergraph product codes} \subset \text{Homological codes} \subset \text{Stabilizer codes}.$$

105 Noted that homological codes belong to mutually orthogonal binary codes, and stabilizer codes belong to
 106 additive self-orthogonal code over GF (4) with respect to the trace Hermitian inner product
 107 **Theorem 1:** it guarantees that from any full-rank classical LDPC parity-check matrix H , you can system-
 108 atically build a quantum LDPC code whose parameters are exactly those given.

Classical	Quantum (constructed)	Notes
Code $[n, k, d]$	$\rightarrow [[n^2 + (n - k)^2, k^2, d]]$	Quantum code parameters
LDPC (sparse)row weight i , column weight j	\rightarrow LDPC (row weight $\approx i + j$)	Sparsity preserved
Parity-check matrix H	$\rightarrow (H_X, H_Z)$ built from $H \otimes I, I \otimes H^T$	CSS-type stabilizers
Distance d	\rightarrow Distance d	Same as classical code
Rate k/n	$\rightarrow \frac{(k/n)^2}{1 + (1 - k/n)^2}$	Quantum rate expression

109 **LDPC codes** linear codes with sparse parity check matrix and can also be described by Tanner graph
 110 denoted by bipartite $\mathcal{T}(V, C, E)$. For $H = \mathbb{F}_2^{r \times n}$, $V = 1, \dots, n$ (called varaiable nodes) is the columns of H and
 111 $C = \otimes_1, \dots, \otimes_r$ (check nodes) with column indices i and row indices j . There is an edge set E when $H_{ij} = 1$
 112 **Generalizations from Toric code** An $m \times m$ toric code (V, E) can be represented as $\mathbb{Z}/m\mathbb{Z} \times \mathbb{Z}/m\mathbb{Z}$, where
 113 the two-dimensional vertex set consists of coordinates (x, y) with each coordinate ranging over $\{0, 1, 2, \dots, m -$

¹¹⁴ 1}. The vertex–edge incidence matrix \mathbf{H}_1 is defined such that $(\mathbf{H}_1)_{ij} = 1$ if vertex i is incident to edge j .
¹¹⁵ Each i -th row of \mathbf{H}_1 corresponds to a vertex (an X -stabilizer), and each j -th column corresponds to an
¹¹⁶ edge, which represents a physical qubit. Pictorially, for a four qubits repetition code (building block of toric
code) can be denoted as in Table 1. Let $H_1 \in \{0, 1\}^{r_1 \times n_1}$ and $H_2 \in \{0, 1\}^{r_2 \times n_2}$ be classical parity-check

X stabilizer (row)	edge ₀	edge ₁	edge ₂	edge ₃
X ₀	1	1	0	0
X ₁	0	1	1	0
X ₂	0	0	1	1
X ₃	1	0	0	1

Table 1: Toric code H_r matrix for 4 edges

¹¹⁷ matrices. Define identity matrices I_a of the indicated sizes, and use the Kronecker product \otimes . Then, the
¹¹⁸ CSS stabilizer matrices are given by
¹¹⁹

$$H_X = [H_1 \otimes I_{n_2} \mid I_{r_1} \otimes H_2^\top], \quad H_Z = [I_{n_1} \otimes H_2 \mid H_1^\top \otimes I_{r_2}].$$

¹²⁰ **Toric code as a special case.** If both classical codes are chosen as the length- L repetition code with
¹²¹ parity-check $H_r \in \{0, 1\}^{L \times L}$ (representing a cyclic ring), then the toric-code stabilizer matrices become

$$H_X = [H_r \otimes I_L \mid I_L \otimes H_r^\top], \quad H_Z = [I_L \otimes H_r \mid H_r^\top \otimes I_L].$$

¹²² Here the rows of H_X correspond to plaquette (face) X -stabilizers and the rows of H_Z correspond to vertex
¹²³ Z -stabilizers, while the columns index the $2L^2$ edge qubits of the lattice.

¹²⁴ 3.3 Logical measurements of Shor and Steane type

¹²⁵ Standard approach will encounter two possible limitations. First, if an error occur on the ancilla qubits, the
¹²⁶ error will propagate to data qubits and cause higher weight errors. Below shows a graph of common error
¹²⁷ propgations extracted from [13]

¹²⁸ Shor’s fault-tolerant logical measurements are implemented by applying transversal gates between data
¹²⁹ qubits and ancilla GHZ (cat) states. The procedure requires multiple rounds, where each GHZ ancilla
¹³⁰ interacts transversally with the data qubits and is then measured in the X (Z) basis, corresponding to initial
¹³¹ input state $|\overline{+}\rangle$ ($|\overline{0}\rangle$).

¹³² These repeated measurements allow one to perform majority voting on the syndrome outcomes, thereby
¹³³ suppressing the effect of measurement errors. Fault tolerance requires that errors arising at any stage do not
¹³⁴ propagate uncontrollably to the data qubits. Figure 2 illustrates this process.

¹³⁵ One potential issue is that ancilla faults during syndrome extraction can propagate in such a way that
¹³⁶ errors mimic measurement errors. To avoid this mixing, each round of syndrome extraction must itself be
¹³⁷ implemented fault-tolerantly. By performing fault tolerant error correction in each state, a single fault can
¹³⁸ only corrupt the outcome and then be fixed during that round. This guarantees that majority voting across
¹³⁹ repeated rounds of cat state measurements produces valid syndrome information.

Shor’s method requires repitions of each stage to alleviate an probability

$$P = \frac{1}{2} - (1 - 2p)^d = \frac{1}{2} - \Delta$$

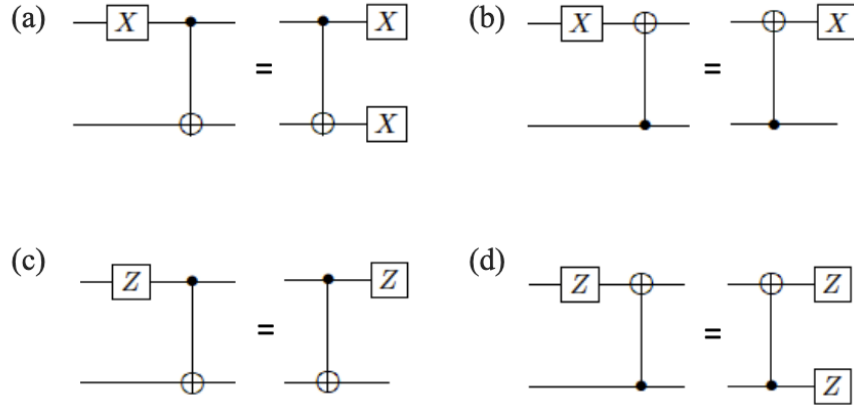


Fig. 3. Propagation of X and Z errors through the CNOT gates.

Figure 1:

¹⁴⁰ of logical error occurs, where p is the single qubit error probability and d is the circuit depth of each stage.
¹⁴¹ The majority vote requires $O(e^{2d})$ repetitions.

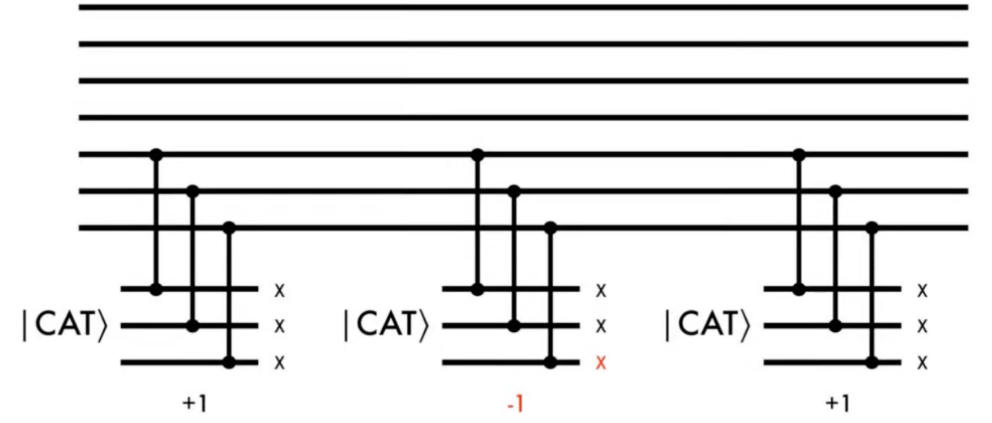


Figure 2:

¹⁴² In Steane method, logical measurement is performed by preparing an ancilla block encoded in the same
¹⁴³ CSS code (e.g., $|0_L\rangle = \frac{1}{\sqrt{2}}(|++\rangle + |--\rangle)^{\otimes 3}$ or $|+_L\rangle$ for the Shor code.) and coupling it to the data
¹⁴⁴ block with transversal CNOTs, realizing

$$\text{CNOT}^{\otimes n} = \overline{\text{CNOT}}^{\otimes k}$$

¹⁴⁵ for an $\llbracket n, k, d \rrbracket$ CSS code. This is in fact mapping the measurement outcome from data code block to ancilla
¹⁴⁶ code block:

¹⁴⁷ Let the data block be $|\psi\rangle = \alpha|0_L\rangle + \beta|1_L\rangle$ and the ancilla be $|0_L\rangle$. After transversal CNOTs: $|\psi\rangle|0_L\rangle \mapsto$
¹⁴⁸ $\alpha|0_L\rangle|0_L\rangle + \beta|1_L\rangle|1_L\rangle$. Measuring the ancilla block in the Z basis reveals the eigenvalue of Z_L on the data
¹⁴⁹ block, while collapsing it into $|0_L\rangle$ or $|1_L\rangle$ accordingly.

Unlike Shor's cat-state method, which measures stabilizers one by one, Steane's method allows all stabilizers of one error type (either X -type or Z -type) to be extracted in a single round. One can imagine that once an measurement error occurs in Steane's parity checks, more parity checks outcome can be used to infer the syndromes compared with Shor's method that require more qubits for multiple stages measurements for one set of syndrome in each stage. The logical error rate yields

$$P = \mathcal{O} \left(p^{\frac{d-1}{2}} \right)$$

150 . Here, d is the code distance.

151 For an general $\llbracket n, k, d \rrbracket$ code, it is easily to generalize the ancilla states to $|0\rangle = \overline{|+_1 \dots 0_i \dots +_k\rangle}$ for a Z
152 type measurements, since $X_j|+_k\rangle$ leaves no change of the state, the measurement of Z_i will only extract
153 information from i qubits (the state $|+_k\rangle$, which treats all Z measurement outcomes on an equal footing).
154 $|0_i\rangle$ is just the ancilla state (measurement state) for Z_i stabilizers. Dimensions of $|0_i\rangle$ state is the weight of
155 Z_i stabilizers. Here, we have noted that for even weight of stabilizers, they are related by local Hadamard
156 gate, called Clifford-equivalent. Also, the choice of codewords are designed by both logical operators and
157 stabilizers. A density matrix for logical state of one-qubit encoding can be found as [1]

$$|0_L\rangle\langle 0_L| = \frac{1}{2^n} (I + \overline{Z}_L) \prod_j (I + S_j).$$

158 For $|1_L\rangle$, one can change the plus sign to minus sign.

159 Problem in Steane code could be ancilla states $|0_L\rangle$ preparation [10]. It can be comprised of a non-fault
160 tolerant preaparation process combined with a verification stage. The verification stage Fig. 3 [3] requires and
161 additional ancilla qubit to flag a successful preparation, like post-process. The whole process then become
162 fault-tolerant but with successful rate e^{-np} , with n being number of gates and p the successtul probability
163 of each gate. For state other than $|0_L\rangle$ can be prepared combined with Clifford operations. Noted that
164 apart from Clifford operations, magic state injection ($T|+\rangle$) is also required to fulfill the universal quantum
165 operations. Similarly, by state distillation or code concatenation, desired ancilla qubit states can be obtained
166 but with large overheads [17].

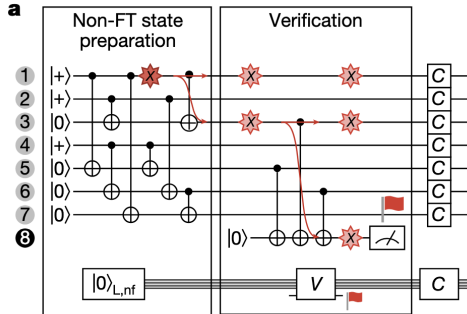


Figure 3:

167 Another trick for ancilla states creation in Steane code is by performing X-type measurements. It seems
168 like we can create the codewords $|0_L\rangle$ by following a state projection from logical operators and stabilizers:

$$\frac{1}{2^J} (I + \overline{Z}_L) \prod_j (I + S_j).$$

169 If we perform X type measurements (mathematically described by above formula, while S_j being Z type

170 measurements can be trivial), the mathematical description of this projecting process can be:

$$|0_L\rangle = \frac{1}{2^{J/2}} \underbrace{(I + \bar{Z}_L)}_{j \in X\text{-type}} \prod_{j \in X\text{-type}} (I + S_j) |0^{\otimes n}\rangle + \underbrace{\frac{1}{2^{J/2}} (I + \bar{Z}_L)}_{j \in Z\text{-type}} \prod_{j \in Z\text{-type}} (I + S_j) |0^{\otimes n}\rangle. \quad (1)$$

171 Noted that Z type measurements and logical Z_L measurement act trivially on $|0^{\otimes n}\rangle$ (They are already
 172 in stabilizer group or commute with stabilizers). The formula requires projective operator which could only
 173 be done unitarily. More explicity, an arbitrary state can be written as combination of projective states with
 174 different observables, hence we could write $|0^{\otimes n}\rangle = \frac{I+S_j}{2}|0^{\otimes n}\rangle + \frac{I-S_j}{2}|0^{\otimes n}\rangle$. This also demonstrate that
 175 Eq. 1 have implicitly selectively choose the projective states $\frac{I+S_j}{2}|0^{\otimes n}\rangle$ with some probability. For Steane
 176 code, this probability is $(\frac{1}{2})^3 = \frac{1}{8}$ for three consecutive projecting process.

177 From $|0^{\otimes n}\rangle = \frac{I+S_j}{2}|0^{\otimes n}\rangle + \frac{I-S_j}{2}|0^{\otimes n}\rangle$, we could infer that the correponding error correction of Z-type
 178 could fix the problem when projecting into wrong states. Hence, the process require further fault-tolerant
 179 error correction (FTEC) following the stabilizers measurement to deterministically generate logical $|0_L\rangle$
 180 state(Above are my current understanding which may not correspond to what paper really trying to convey.).
 181 There is no need post-selection for Steane's ancilla qubit preparation as claimeed in the video for logical
 182 qubits number $k = 1$. Also, for $k > 1$ the process can be used to generate $|0^{\otimes k}\rangle$ (all Z measurement at
 183 once) but not $|+1\dots0_i\dots+k\rangle$ (If we want particular Z_i measurement). The reason is that $|+1\dots0_i\dots+k\rangle$ are
 184 not easily prepared anymore. This may make the whole preparation process as hard as directly measuring
 185 logical operators in data block.

186 A natural thoughts then will be can a new choice of ancilla code such that it can achieve a LDPC
 187 measurement on particular logical qubit. The next question is, is there any other choices of ancilla code to
 188 achieve non-postselection, no repition like Steane's method for an $[[m,1,d]]$ (Steane ancilla code: $[[n,1,d]]$ or
 189 $[[n, k ,d]]$)ancilla code. Here, the speaker aims to build a new code that could perform with $m < d$ that
 190 could be more resource freindly.

191 The speaker introduced a measurement process called *homomorphic measurement*. A toric code is an

$$[[n, k, d]] = [[2L^2, 2, L]]$$

192 defined on a torus, which can be represented as a square sheet with periodic boundary conditions. The
 193 stabilizers all commute, and the corresponding logical operators are shown in Fig. 10. The horizontal loops
 194 \bar{X}_1, \bar{Z}_2 and the vertical loops \bar{Z}_1, \bar{X}_2 correspond to logical operators that wrap around the torus in the
 195 horizontal or vertical directions.

196 3.4 Binary vector spaces

197 They construct the homomorphism between data qubits and the ancilla qubits by using CSS codes chain
 198 complexes.

199 An $r \times n$ binary matrix defines a linear map

$$H : \mathbb{F}_2^n \rightarrow \mathbb{F}_2^r,$$

200 where $\mathbb{F}_2 = \{0, 1\}$ with addition and multiplication modulo 2. The transpose H^T is the $n \times r$ matrix with
 201 rows and columns swapped. The kernel (null space) is

$$\ker(H) = \{v \in \mathbb{F}_2^n : Hv = 0\},$$

202 the image (column space) is

$$\text{im}(H) = \{Hv : v \in \mathbb{F}_2^n\},$$

203 and the row space is the span of the rows of H , denoted $\text{rs}(H)$. Note that $\dim(\text{im}(H)) = \dim(\text{rs}(H)) =$
 204 $\text{rank}(H)$.

205 Given a finite set S , the vector space $\mathbb{F}_2[S]$ consists of all formal binary sums of elements in S ,

$$v = \sum_{e \in S} v_e e, \quad v_e \in \mathbb{F}_2,$$

206 which can be naturally identified with subsets of S (element e is present if $v_e = 1$). If $H : \mathbb{F}_2[A] \rightarrow \mathbb{F}_2[B]$,
207 then the transpose defines a map $H^T : \mathbb{F}_2[B] \rightarrow \mathbb{F}_2[A]$ under the corresponding bases.

208 As an example, consider

$$H = \begin{bmatrix} 1 & 0 & 1 \\ 0 & 1 & 1 \end{bmatrix}.$$

209 The image is spanned by the columns $(1, 0)^T$, $(0, 1)^T$, and $(1, 1)^T$, which generate all of \mathbb{F}_2^2 . The row space
210 is spanned by $(1, 0, 1)$ and $(0, 1, 1)$, giving the subspace

$$\{(0, 0, 0), (1, 0, 1), (0, 1, 1), (1, 1, 0)\} \subseteq \mathbb{F}_2^3.$$

211 In the language of quantum error correction, the row space $\text{rs}(H)$ often corresponds to the stabilizer
212 group (constraints on codewords), the image $\text{im}(H)$ corresponds to possible syndrome outcomes, and the
213 kernel $\ker(H)$ corresponds to valid codewords with no detected error.

214 A CSS code with stabilizer X type and Z type will have corresponding stabilizer group isomorphic to
215 $\text{rs}(H_X)$ and $\text{rs}(H_Z)$.

216 The quantum code can be described using two families of Pauli stabilizers. The X -type stabilizer group
217 corresponds to parity checks that involve X operators, and it is isomorphic to the row space of H_X . Similarly,
218 the Z -type stabilizer group corresponds to parity checks that involve Z operators, and it is isomorphic to
219 the row space of H_Z .

220 The X -type logical operators are elements of $\ker(H_Z)$ (like centralizer), meaning they commute with all
221 Z -type checks and therefore preserve the Z -stabilizer constraints. Likewise, the Z -type logical operators are
222 elements of $\ker(H_X)$, since they commute with all X -type checks since a logical operator will stay in the
223 codespace.

224 The number of encoded logical qubits is the number of independent logical degrees of freedom that remain
225 after imposing all stabilizer constraints:

$$k = \dim(\ker(H_X)/\text{rs}(H_Z)) = \dim(\ker(H_Z)/\text{rs}(H_X))$$

226 (quotient subgroup: The elements of the quotient space V/W are the cosets of W . Each coset is of the
227 form $v + W$ for some $v, w \in V$. Algebraically, forming the quotient space V/W , V/W means we treat all
228 vectors that differ by an element of W as equivalent. Topologically, V/W is like shrinking W space into a
229 point. It is also like finding logical qubits dimension using $\dim(2^n/2^{n-k}) = k$). This formula says that logical
230 qubits live in the space of operators that preserve one type of stabilizer (the kernel) but are not redundant
231 with the other type (the row space). The X distance d_X measures how resilient the code is against bit-flip
232 (X -type) errors: it is the minimum number of qubits that must be flipped to implement a nontrivial logical
233 X operation. Formally,

$$d_X := \min\{|c| : c \in \ker(H_Z) \setminus \text{rs}(H_X)\}.$$

234 Similarly, the Z distance d_Z quantifies protection against phase-flip (Z -type) errors:

$$d_Z := \min\{|c| : c \in \ker(H_X) \setminus \text{rs}(H_Z)\}.$$

235 Finally, the overall *code distance* is

$$d = \min\{d_X, d_Z\},$$

236 which sets the maximum number of arbitrary single-qubit errors the code can reliably detect and correct.
237 Physically, the larger the distance, the more robust the code is against noise.

238 Quantum error correction uses this framework because stabilizers operators naturally form abelian groups
239 modulo phases (self-commute).

240 3.5 Algebraic Topology

241 Notes from the lecture [3], the **2-dimensional disk** is defined as

$$D^2 = \{(x, y) \in \mathbb{R}^2 \mid x^2 + y^2 \leq 1\}.$$

242 It consists of all points in the plane whose distance from the origin is less than or equal to 1. **Interior and boundary**

$$\text{Int}(D^2) = \{(x, y) \in \mathbb{R}^2 \mid x^2 + y^2 < 1\}, \quad \partial D^2 = \{(x, y) \in \mathbb{R}^2 \mid x^2 + y^2 = 1\} = S^1. (\partial D^n = S^{n-1})$$

244 **Topological Meaning** In a CW complex, D^2 serves as a **2-cell**. Attaching a 2-cell means gluing a copy of D^2 along its boundary S^1 via a continuous map:

$$f : S^1 \rightarrow X^1.$$

246 For example:

- S^2 is formed by attaching one D^2 to a point ($X^1 = X^0$ here, one D^0 zero D^1 , one $D^2]$, $\chi(S^2) = 2$ (χ defined below)) .
- A torus T^2 is formed by attaching D^2 along a loop that winds in two directions (X^0 : a point, X^1 add two D^1 lines, $f : \partial D^1 = S^0 \rightarrow X^0$. X^2 : add a D^2 two dimensional disk $f : S^1 \rightarrow X^1$) ($X^2 : ab^{-1}a^{-1}b$, the direction of loop are glued will result in different shape, if $X^2 : ab^{-1}ab$ is a Klein bottle). $\chi(T^2) = 0$

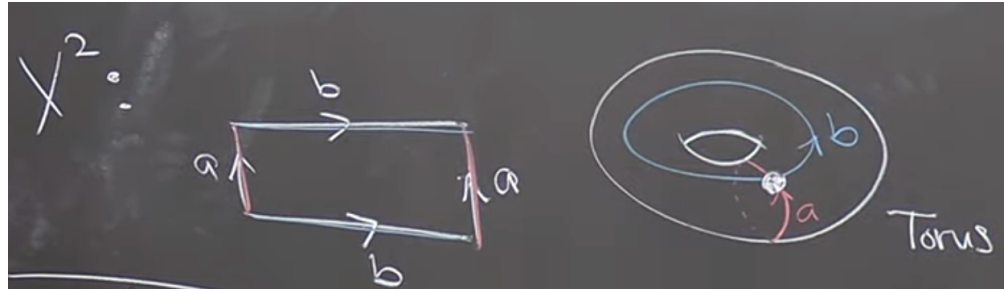


Figure 4: S^1 for torus. X^1 : add

252 **Generalization** The n -dimensional disk is

$$D^n = \{(x_1, \dots, x_n) \in \mathbb{R}^n \mid x_1^2 + \dots + x_n^2 \leq 1\},$$

$$f : S^{n-1} \rightarrow X^{n-1}.$$

254 **Euler characteristic** Vertices $D^0 = V$, Edges $D^1 = E$, Faces $D^2 = F, \dots$

$$\chi = \#\text{even dim}(D) - \#\text{odd dim}(D)$$

$$\chi(T^2) = V - E + F = 1 - E + 1 = 0 \Rightarrow E = 2$$

255 or a torus can be build from $V = 4$, $E = 8$, $F = 4$ and similar goes for S^2 but with χ fixed.

257 **Product and homology.** Noted that D^n is contractible and S^n are not.

258 **homotopy \simeq**

Spaces (X, Y)	Relationship	Intuition
D^n and a point $*$	$D^n \simeq *$	A disk can be shrunk to a point (contractible).
S^1 and a circle-shaped wire loop	$S^1 \simeq$ any loop	All circles have the same homotopy type
S^1 and a torus (T^2)	Not homotopy equivalent	A torus has more “holes.”
\mathbb{R}^n and a point	$\mathbb{R}^n \simeq *$	Can contract the entire space to a point.
A hollow cylinder and a circle	$S^1 \times I \simeq S^1$	The cylinder retracts onto its circular core.

259 The torus (solid torus: $D^2 \times S^1$) is defined as $T^2 = S^1 \times S^1$ and its *fundamental group* is $\pi_1(T^2) \cong \mathbb{Z} \times \mathbb{Z}$.

260 In contrast, for the circle we have $\pi_1(S^1) \cong \mathbb{Z}$. Since the integer group \mathbb{Z} is not isomorphic to the product group $\mathbb{Z} \times \mathbb{Z}$, it follows that $T^2 \not\simeq S^1$. Geometrically, if one tries to shrink the torus T^2 into a circle S^1 , one must collapse or “break” one of the gluing directions that form T^2 . Since this cannot be done continuously without tearing the surface, T^2 and S^1 are not homotopy equivalent. $D^1 \times D^2$: a solid cylinder (sphere)

264 Some identities:

$$D^n \times D^m = D^{n+m}$$

$$\partial(X \times Y) = (\partial X \times Y) \cup (X \times \partial Y)$$

265 \cup is called union. For example, calculate $\partial(D^2 \times [1, 0]) = (\partial D^2 \times [1, 0]) \cup (D^2 \times \partial[1, 0]) =$

266 $(S^1 \times [1, 0]) + D^2 \times \{0, 1\}$ It is exactly the surface of the cylinder. Or simply, $\partial(D^2 \times [1, 0]) = \partial D^3 // = S^2$

267 So calculate $\partial(S^1 \times S^1 \times [1, 0]) = S^1 \times S^1 \times \{0, 1\}$ is two copies of torus surface.

268 Another example: $S^3 = \partial(D^4) = \partial(D^2 \times D^2) = S^1 \times D^2 \cup D^2 \times S^1$ (two tori formed by looping around different directions, pictorially, draw S^1 first for first qubit and then draw D^2 connected on S^1 similar for second torus but with opposite order.). Union can be think of gluing, hence gluing two tori is S^3 .

271 Examples of **Quotients** in topology: $D^1/S^0 = S^1$, $D^2/S^1 = S^2$, $S^2/S^1 = S^1 \vee S^1$, \vee (pronounce: wedge), also examples in Fig. 5

273 **Homology group** is used to describe

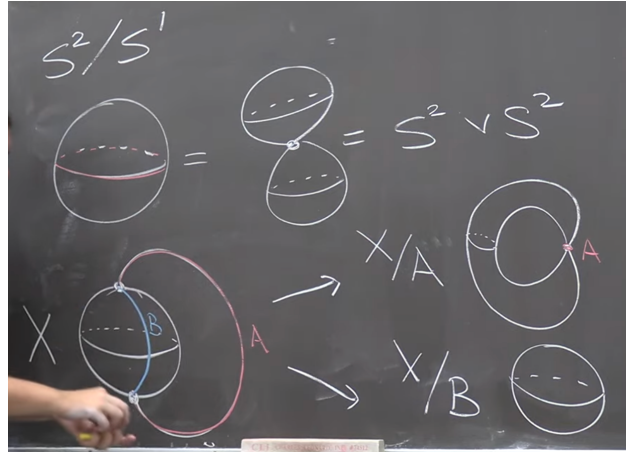


Figure 5:

274 3.5.1 Homology Groups

275 Vector spaces over \mathbb{F}_2 are abelian groups C_i under addition. Boundary operators ∂_i are group homomorphisms (Like in toric code, logical Z_L is noncontractible loops around the torus.). Groups here are in topological

277 sense not the same as Stabilizers group in physical Pauli sense. A chain complex is just a sequence of abelian
278 groups with compatible homomorphisms, typically written as

$$C_2 \xrightarrow{\partial_2} C_1 \xrightarrow{\partial_1} C_0, \quad \text{with } \partial_1 \circ \partial_2 = 0.$$

279 In CSS codes, $H_X = \partial_1$ and $H_Z^T = \partial_2$ naturally satisfy $H_X H_Z^T = 0$ is the stabilizers. The above
280 **homology group** is used to describe data qubits C_1 and logical operators ($\ker(\partial_1)/\text{im}(\partial_2)$)

281 Logical operators are homology classes H_i . They are cycles Z_n (commute with stabilizers) but not
282 boundaries B_n themselves (not product of stabilizers). Mathematically:

$$H_n = Z_n / B_n \tag{2}$$

$$Z_n := \ker \partial_n := \{ c \in C_n \mid \partial_n(c) = 0 \} \tag{3}$$

$$B_n := \text{im } \partial_{n+1} := \{ \partial_{n+1}(c) \mid c \in C_{n+1} \} \tag{4}$$

283 This correspond to $\dim(\ker(\partial_n)/\text{im}(\partial_{n+1})) = \dim(\ker(H_Z)/\text{rs}(H_X)) = k$. The algebra links with Fig. 10 toric
284 code. The toric code can be expressed as the chain complex $C_2 \xrightarrow{\partial_2} C_1 \xrightarrow{\partial_1} C_0$, where qubits live on edges
285 (C_1), X -stabilizers are associated with vertices (C_0), and Z -stabilizers with faces (C_2). The logical operators
286 are characterized by the first homology group

$$H_1 = \ker(\partial_1) / \text{im}(\partial_2) \cong \mathbb{Z}_2 \oplus \mathbb{Z}_2 = (0,0), (1,0), (0,1), (1,1),$$

287 which corresponds to the two nontrivial loops around the torus that encode the logical qubits, while torus
288 requires two loops to decribe its topology. In general,

$$\ker(\partial H_Z) / \text{im}(\partial H_X)$$

289 corresponds to the X -type logical operators, while

$$\ker(\partial H_X) / \text{im}(\partial H_Z)$$

290 corresponds to the Z -type logical operators. Pictorially, one can imagine that all closed loops of errors on
291 qubits in Fig. 10 lie in $\ker(\partial H_Z)$, but many of them can also be formed as products of X stabilizers. The
292 only exceptions are loops that connect opposite edges (loop around) of the torus, which give nontrivial errors
293 that cannot be detected and by design act as logical Z operators.

294 3.6 Homomorphic logical measurements

295 As we have elaborated on Shor and Steane measurement downsides and limitations, here we dorectly go
296 to the arthor main points, homomorphic logical measurements. They are trying to find a new code $[[m, 1
297,d]]$ that could unify or improve before mentioned downsides. The process first start from preparing 1.
298 preparing ancilla in $|0^{\otimes k}\rangle$ 2. perform interaction Γ between ancilla and data block. 3. measured Z basis on
299 ancilla block.

300 Data–Ancilla Interaction

301 Applying the homomorphism for CSS codes into their ancilla code construction by considering possible
302 interaction between data-ancilla interaction (typically utlising similar mathematical but applying on different
303 purposes.):

304 We have two CSS codes: - Data: (H_X, H_Z) of length n , - Ancilla: (H'_X, H'_Z) of length m . Before interaction,
305 stabilizer groups are written as

$$T_Z = \text{rs} \begin{pmatrix} H_Z & 0 \\ 0 & H'_Z \end{pmatrix}, \quad T_X = \text{rs} \begin{pmatrix} H_X & 0 \\ 0 & H'_X \end{pmatrix}.$$

306 After Interaction (Γ a gate matrix $\Gamma : \mathbb{F}_2^m \rightarrow \mathbb{F}_2^n$ (CNOTs)), stabilizer groups can be written as

$$T'_Z = \text{rs} \begin{pmatrix} H_Z & 0 \\ H'_Z \Gamma^T & H'_Z \end{pmatrix}, \quad T'_X = \text{rs} \begin{pmatrix} H_X & H_X \Gamma \\ 0 & H'_X \end{pmatrix}.$$

307 To explain T'_Z further, it is like the outcome of H'_Z on ancilla qubits, is determined not only by the state
 308 initial state $|0_L\rangle$ lie in ancilla block but also $H'_Z \Gamma^T$ when performing interaction, which is like a different
 309 mapping other than Steane style, from my understanding, Steane style measurement follows $H'_Z \Gamma^T = H'_Z$
 310 (Since Γ here is like identity for transversal gates in Steane measurement) and also $H'_Z = H_Z$ since they
 311 are using same logical codewords, hence same stabilizers. Just like the author mentioned, for Shor's style
 312 measurment, $H'_Z \neq H_Z$ since H_Z should correspond to cat states stabilizers (1D).

313 The role interchange between target and controlled of X type and Z type errors can be explained by the
 314 error propagation shown in Fig. 6.

315 We also required conditions such $T'_Z = T_Z$, $T'_X = T_X$, i.e.

$$\text{rs}(H'_Z \Gamma^T) \subseteq \text{rs}(H_Z), \quad \text{rs}(H_X \Gamma) \subseteq \text{rs}(H'_X).$$

316 This ensures the interaction preserves the stabilizer groups.

317 **Definition (Homomorphic gadget).** An $[[n, k, d]]$ homomorphic gadget (H'_X, H'_Z, Γ) for an $[[n, k, d]]$
 318 CSS code (H_X, H_Z) consists of: (i) an ancilla $[[m, k', d']]$ CSS code with checks (H'_X, H'_Z) ; (ii) a gate matrix
 319 $\Gamma : \mathbb{F}_2^m \rightarrow \mathbb{F}_2^n$; such that

$$\text{rs}(H'_Z \Gamma^T) \subseteq \text{rs}(H_Z), \quad \text{rs}(H_X \Gamma) \subseteq \text{rs}(H'_X). \quad (5)$$

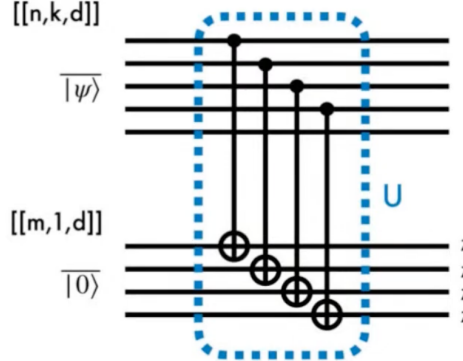


Figure 6:

320 To summarize, a stabilizer element (in fact also logical error) $v \in \ker H'_Z$ are transformed as $\Gamma v \oplus v$, acted
 321 on data block (Γv) and ancilla block (v), since ancilla state is prepared in logical $|0^{\otimes k}\rangle$, the outcome will be
 322 Γv . There are two cases: where $v \in \text{rs}(H'_Z)$ or $v \notin \text{rs}(H'_Z)$, the former under homomorphic gadget setting
 323 will preserve the structure of $v \in \text{rs}(H'_Z)$ and act as a X error detection for data block. The latter are in
 324 fact mapping logical Z operation into ancilla block. As mentioned, the outcome will be Γv (it is measured
 325 in ancilla block but in fact bring based on data block information. One can simply assume a vector acting
 326 by matrix T'_Z to see this) which will isomorphic to $\Gamma \ker(H_X)$ (seems might encounter vector space outside
 327 $\Gamma \ker(H_X)$)

3.7 Homomorphic measurements on surface codes

329 Surface codes are defined as cellulations of a manifold $\mathcal{M} = (\mathcal{V}, \mathcal{E}, \mathcal{F})$, where the boundary maps $\partial_2 : \mathcal{F} \rightarrow \mathcal{E}$
 330 and $\partial_1 : \mathcal{E} \rightarrow \mathcal{V}$ obey the CSS code condition $\partial_1 \partial_2 = 0$. (Can LDPC CSS codes, such as hypergraph product
 331 codes, have different homomorphic gadgets?) Linear maps $\gamma : \mathcal{A} \rightarrow \mathcal{D}$ connect the ancilla and data surface

332 codes. In fact, the gate matrix is given by $\Gamma = \gamma_1$ in the paper, where $\gamma_1 : \mathcal{E}' \rightarrow \mathcal{E}$ is the linear map between
 333 qubits. The data and ancilla surface codes are defined respectively as $\mathcal{D} = (\mathcal{V}, \mathcal{E}, \mathcal{F})$, and $\mathcal{A} = (\mathcal{V}', \mathcal{E}', \mathcal{F}')$.
 334 Explicitly, the relation between data block and ancilla block:

$$\begin{array}{ccccc} \mathbb{F}_2[\mathcal{F}'] & \xrightarrow{\partial'_2} & \mathbb{F}_2[\mathcal{E}'] & \xrightarrow{\partial'_1} & \mathbb{F}_2[\mathcal{V}'] \\ \downarrow \gamma_2 & & \downarrow \gamma_1 & & \downarrow \gamma_0 \\ \mathbb{F}_2[\mathcal{F}] & \xrightarrow{\partial_2} & \mathbb{F}_2[\mathcal{E}] & \xrightarrow{\partial_1} & \mathbb{F}_2[\mathcal{V}] \end{array}$$

335 The above relation naturally gives homomorphic gadget conditions shown in Eq. 5, as $\gamma_1 \partial'_2 = \partial_2 \gamma_2 \subseteq \partial_2$ and
 336 $\gamma_0 \partial'_1 = \partial'_1 \gamma_1 \subseteq \partial_1$. The paper seems like weakening the global homeomorphism constraints of a usual linear
 337 map $\Gamma(\gamma_i)$ such as Steane or Shor to local homeomorphism. This generalization gives more degree of freedom
 338 to represent logical operators to a single non-contractable loop in a new manifold. This generalization do
 339 not preserve transversal gates, as we can see that γ_i local homeomorphism, or covering spaces can be many-
 340 to-one linear maps. There are also certain boundaries for manifold M , with two rough boundaries and two
 341 smooth boundaries is the planar surface codes [4].

342 The paper constructs homomorphic gadgets into two categories: **subspaces of data code space** \mathcal{D} and
 343 **covering space** of \mathcal{D} . For the first one, it is natural that homomorphic gadget can be constructed given Γ
 344 is injective (one-to-one, hence transversal and fault tolerant. $\mathcal{A}(\mathcal{V}', \mathcal{E}', \mathcal{F}') \in \mathcal{D}(\mathcal{V}, \mathcal{E}, \mathcal{F})$). Shor code can be
 345 thought of as $A = l \subseteq (\mathcal{V}, \mathcal{E})$ and l loops not intersecting (loops here generally mean logical operators, so
 346 not restricted on toric code loops, if loop intersects, it could involve two logical operators which is not in cat
 347 state gadget.), with $F = \emptyset$ and this indicates repetition code $0_L = \frac{1}{\sqrt{2}}(|+++... \rangle + |---... \rangle)$ will have only
 348 X stabilizers, for repetition code of Z stabilizers, one use T'_X which interchange the controlled and target
 349 qubits between data and ancilla qubits.

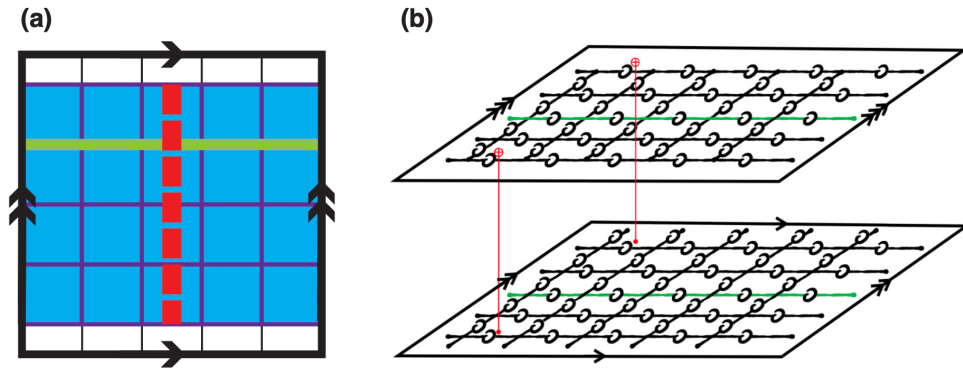


Figure 7:

350 Fig. 7 (a) describes a toric code \mathcal{D} and the blue region describes surface code with smooth boundaries.
 351 Red line connecting two boundaries are then logical X (or by seeing red lines crossing sets of Z stabilizers.).
 352 The logical operator dimension of \mathcal{A} are then reduced from four (complete mapping correspond to Steane
 353 measurement) to two. This ensures simpler preparation of ancilla states as mentioned in 3.3, which is also a
 354 problem associated with Steane measurement if utilising a complete mapping between data (might involve
 355 two or more logicals) and ancilla block.

356 Here we move on to homomorphic gadgets from **covering spaces**. Emphasizing the motivation again,
 357 if we want to perform a single-shot nondestructive logical CSS measurements on multiple logical operators
 358 (ancilla block), then the direct mapping such as Steane code or $A \in l$ inevitably support two logicals degree
 359 of freedom but with overlapped qubits, furthermore, multiple logical qubits ancilla is hard to prepare. The

360 idea is to unfold the manifold to make logical operators uniquely represented by a non-intersecting loop in
 361 ancilla sheets. This resolves all of the problems mentioned.

362 **Groups acting on spaces:** The infinite *simply connected* covering space U (for example, \mathbb{R}^2) is equipped
 363 with a regular tiling (cellulation: divided into cells like vertices, edges, faces, $[i, i+1] \times [j, j+1]$ for $(i, j) \in \mathbb{Z}^2$).
 364 A group G of symmetries (leave the grid-structure intact), such as translations or rotations, acts on U , and
 365 for each point $u \in U$, its orbit $Gu = \{g(u) \mid g \in G\}$ consists of all symmetry-related copies of u (all Gu
 366 collapses to one point.). The orbit space U/G is the corresponding quotient manifold (for instance, a torus),
 367 and the quotient map (continuous and open) $p_G : U \rightarrow U/G$ sends each point u to its orbit Gu . The resulting
 368 manifold $M = U/G$ is the compact surface on which the surface code is defined. Because each element of G
 369 preserves the tiling of U , the quotient map p_G induces a cellulation of M ; that is, every k -cell in U maps to
 370 a k -cell in M , preserving the lattice structure.

371 As discussed in Sec. 3.5 and illustrated in Fig. 4, one can regard the **first example: torus** as the
 372 quotient of the real plane $\mathcal{U} = \mathbb{R}^2$ by the integer translation group $G \cong \mathbb{Z} \times \mathbb{Z}$
 373 (translations $t_{r,s}(x, y) : (x, y) \rightarrow (x + dr, y + ds)$ for an $[2d^2, 2, d]$ toric code). Intuitively, this corresponds to
 374 identifying points that differ by integer shifts, i.e., taking 0 and 1 as the same point in each direction. The
 375 quotient $\mathbb{R}^2 / (\mathbb{Z} \times \mathbb{Z})$ can thus be represented by the unit square $[0, 1] \times [0, 1]$, where opposite edges—labeled
 376 a and b in Fig. 4—are glued together to form the torus topologically. Because the torus is constructed as
 377 this quotient, its *fundamental group* is isomorphic to the translation group itself,

$$\pi_1(T^2) \cong \mathbb{Z} \times \mathbb{Z},$$

378 with each generator corresponding to one of the two noncontractible loops along the a and b directions.

379 We can also consider **second example: hyperbolic surface codes**, with the universal $\mathcal{U} = \mathbb{H}^2$ which
 380 are defined on regular tilings characterized by a Schläfli symbol $\{r, s\}$ (note that this is unrelated to the
 381 integer coordinates (r, s) used earlier). Here, r indicates that each face (tile) is a regular polygon with r
 382 sides, and s means that s such faces meet at each vertex. The pair $\{r, s\}$ determines both the curvature of
 383 the surface and the stabilizer structure: if $(r - 2)(s - 2) < 4$, the surface is spherical; if $(r - 2)(s - 2) = 4$,
 384 it is Euclidean (flat, as in the toric code); and if $(r - 2)(s - 2) > 4$, it is hyperbolic. In the code, each
 385 Z -type stabilizer acts on r qubits (around a face), and each X -type stabilizer acts on s qubits (around a
 386 vertex). The **Coxeter group** $G_{r,s}$ preserve the tiling structure. Group G is chosen as the normal subgroup
 387 of $G_{r,s}$ (like relation between Pauli group and Clifford group). The parameters $\llbracket n, k, d \rrbracket$ satisfy $k = O(n)$
 388 and $d = O(\log n)$.

389 (This passage formalizes how one can form a quotient manifold \mathcal{U}/G by identifying points under a group of
 390 **local homeomorphism**, in a way that preserves the cellulation and thus the qubit and stabilizer structure
 391 of the original topological code.)

392 The *image* of N_u , $g(N_u)$ is the set of all points in \mathcal{U}/G that are reached when applying the map p_G to every
 393 point in $N_u : p_G(N_u) = \{p_G(x) \mid x \in N_u\}$. Therefore, if N_ν is a small open patch around u in the original
 394 space \mathcal{U} , then the set $N_\nu := p_G(N_\nu)$ is the corresponding small open patch and disjoint in the quotient space
 395 \mathcal{U}/G . N_ν and $g(N_u)$ are homeomorphic. Also, no nontrivial $g(u) = u$ (Not fixed points mean mapping all
 396 of the points to N_ν , bijective: injective and surjective)

397 **Third example: $[2d^2, 2, d]$ toric code.** if we choose U_u for any $u = (x, y) \in \mathcal{U} = \mathbb{R}^2$

398 The *lifting property* is the key topological feature they rely on, since it allows any logical operator—
 399 represented by a noncontractible loop on the base surface to be lifted to a non-self-intersecting path on a
 400 multi-sheeted covering manifold. The loop on \mathcal{U} starts at u and ends at some translated copy of $g(u)$.

401 **Fourth example: $[2d^2, 2, d]$ toric code.** Lifting a horizontal loop l on \mathcal{U}/G to \tilde{l} . Mathematically,
 402 denoted as $g(u) = t_{1,0}(u)$, where $u = (0, 0) \in \mathcal{U}$. One can imagine logical operator correspond to \mathcal{U}/G is like
 403 viewing $(0, y)$ and (d, y) as same point. Also, \tilde{l} is guaranteed to be a loop if and only if l is contractible on
 404 \mathcal{U}/G given U is simply connected.

405 Consider another covering map $p_G^H : \mathcal{U}/H \rightarrow \mathcal{U}/G$ defined as $p_G^H H(u) = G(u)$. When $H = \langle t_{1,0} \rangle$
 406 (horizontal translations), the intermediate covering space \mathcal{U}/H is an infinite *cylinder*, obtained by identifying
 407 points along the horizontal direction of the universal cover $U = \mathbb{R}^2$. The base space \mathcal{U}/H , where $G =$
 408 $\langle t_{1,0}, t_{0,1} \rangle$, is the *torus*, obtained by identifying both horizontal and vertical directions. On the torus \mathcal{U}/H ,

409 the horizontal and vertical logical loops correspond to $t_{1,0}$ and $t_{0,1}$, respectively. When lifted to the cylinder
 410 \mathcal{U}/H , the horizontal loop remains closed since $t_{1,0} \in H$, while the vertical loop becomes an open segment as
 411 $t_{0,1} \notin H$. This pictorizes the general relation

$$g \in H \iff \text{the lifted loop } \ell \text{ is closed on } \mathcal{U}/H.$$

412 **Fifth example:** $[[2d^2, 2, d]]$ toric code is same as the previous example for relation
 413 $g \in H \iff \text{the lifted loop } \ell \text{ is closed on } \mathcal{U}/H.$

414

415 3.8 Homomorphic gadgets for covering spaces

416 Now we can start to construct homomorphic gadgets for covering spaces. Until now, we make some remarks:
 417 $g(u)$ lives in \mathcal{U} and $p_G(g(u)) = p_G(u)$ on \mathcal{U}/G but $g(u) \neq u$ on \mathcal{U} could
 418 be possible. This coule directly be seen $p_G(u) = Gu = \{g(u) \mid g \in G\}$ while p_G represented all possible
 419 $g(u) \in \mathcal{U}$ and collapse to one point in space \mathcal{U}/G by definition.

420 The task is to find $\mathcal{A} \subseteq \tilde{D} = \mathcal{U}/H$ (where H is defined previously) such that $\mathcal{A} \subset l'$ and satisfies $d_{\mathcal{A}} = d_{\mathcal{D}}$.

421 As discussed before, the subgroup $H \supseteq G$, and $p = p_G^H$ is the covering map from \mathcal{U}/H to \mathcal{U}/G . If we pick
 422 $H = \langle g \rangle$ ($g \in G$), then all the loops are unfolded except the loop l corresponding to the g -translation.

423 Specifically, we map two non-contractible loops to one non-contractible loop in the ancilla block $A \subseteq$
 424 $\tilde{D} = \mathcal{U}/H$. This ensures that we only have one unique logical operator in \mathcal{U}/H , where H is chosen to be
 425 $\langle t_{1,1} \rangle$ (i.e., no overlapping qubits like in the toric code with different logicals). This unique logical operator
 426 can be designed to represent $\overline{Z_1 Z_2}$, enabling single-shot measurement. Noted that ancilla block \mathcal{A} is chosen
 427 such that $d_A = d_D$ (minimum weight of a nontrivial X logical operator of \mathcal{A} , is the red line part in Fig. 9(c)

428 The induced homomorphic gadget (not necessarily transversal for covering maps) is induced by map
 429 $\gamma := p \circ \tilde{\gamma}$, where $\tilde{\gamma} : \mathcal{A} \rightarrow \tilde{D}$, $\gamma : \mathcal{A} \rightarrow \mathcal{D}$

430 One can obtain a clearer physical picture from Fig. 8. Panel (a) shows the data-qubit manifold $\mathcal{U}/G = \mathbb{T}^2$,
 431 where the green loops represent the logical operators $Z_1 Z_2$. In panel (b), the corresponding logical loop ℓ
 432 is lifted to the covering space \mathcal{U} , forming a path that connects the two points (x, y) and $(x + d, y + d)$
 433 (connecting two grids), pictorially, imagine two grids collapse into one grid due to translation symmetry,
 434 then the green lines in Fig. 9(b) become Fig. 9(a). Finally, panel (c) illustrates the ancilla-qubit manifold
 435 \mathcal{U}/H , with $H = \langle t_{1,1} \rangle$ which takes the form of a cylinder. The covering spaces correspond to Fig. 9(c) is
 436 shown in Fig. 8. Noted that red line in Fig. 9(c) is logical X operator, when depicting in Fig. 8, it will
 437 become a line connected two smooth boundaries.

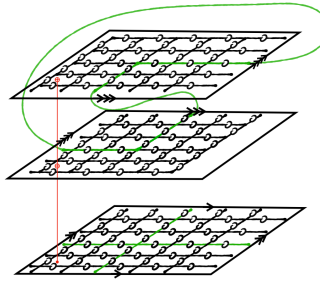


Figure 8:

438 3.9 Fault tolerance

439 Since there is no transversal mapping for $\gamma := p \circ \tilde{\gamma}$, while homeomorphism between data sheets and ancilla
 440 sheets in standard measurement method is levergaed to local homeomorphism between them. The mapping

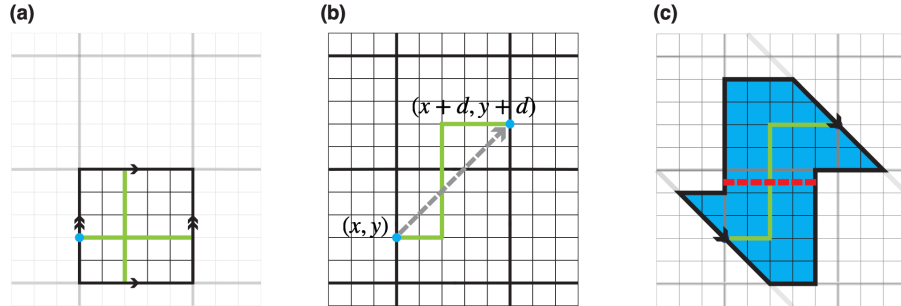


Figure 9: (a) Data-qubit manifold $\mathcal{U}/G = \mathbb{T}^2$, where the green loops represent the logical operators Z_1Z_2 . (b) The covering space \mathcal{U} , showing the lifted path connecting (x, y) and $(x + d, y + d)$. (c) The ancilla-qubit manifold \mathcal{U}/H , which is topologically equivalent to a cylinder.

441 between edges then might encounter many-to-one coupling, $\gamma_1^T(e) \in E'$. Even under these correlations, it is
442 shown it still have fault tolerance with X error $\min\{d_{\mathcal{A}}, d_{\mathcal{D}}\}$.

443 3.10 Joint measurement

444 Considering two disjoint loops l_1 and l_2 on \mathcal{U}/G , if the manifold \mathcal{M} is path connected, then logical operator
445 can be $l_1 p l_2 p^{-1}$.

446 For two separate codes, say two ancilla blocks $\mathcal{A}_1, \mathcal{A}_2$, in order to prepare ancilla, one uses a lattice
447 surgery approach to entangle two blocks from the initial state $|+\rangle_1|+\rangle_2$ into the logical Bell state $|+\rangle_L = \frac{1}{\sqrt{2}}(|00\rangle + |11\rangle)$ by measuring $Z_{\mathcal{A}_1}Z_{\mathcal{A}_2}$ with some surface code A' satisfying $\partial A' = l'_1 \cup l'_2$. (Note that the
448 results will be either $|+\rangle_L = \frac{1}{\sqrt{2}}(|00\rangle + |11\rangle)$ or $|-\rangle_L = \frac{1}{\sqrt{2}}(|01\rangle + |10\rangle)$. One then applies X_1 for correction.)
449 Just like the layer of ancilla blocks depicted in Fig. 8, $Z_{\mathcal{A}_i}$ can be a closed loop on the boundary, $l'_i \subseteq \partial \mathcal{A}_i$.
450 After ancilla preparation, one could construct homomorphic gadget (entangle data block and ancilla block)
451 and perform logical measurement afterwards. Ancilla states can be prepared *offline*.
452

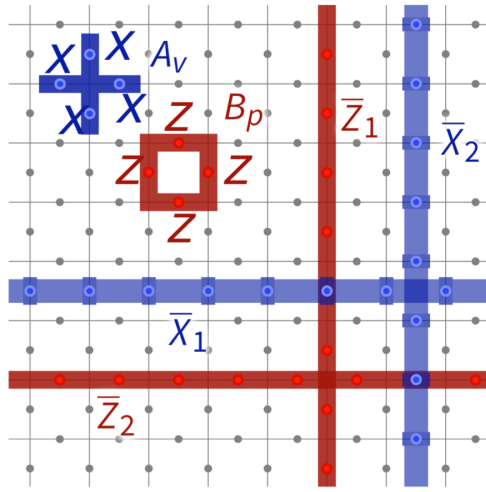


Figure 10:

453 **4 Summary**

454 They first establish the algebraic conditions under which the interaction matrix $\Gamma = \gamma_1$ between a data
455 block $\llbracket n, k, d \rrbracket$ and an ancilla block $\llbracket n', k', d' \rrbracket$ preserves the stabilizer structure. Motivated by topological
456 intuition, the authors represent intersecting logical loops as a single noncontractible loop. This construction
457 achieves two goals: (1) it enables single-shot measurement of multiple logical operators, and (2) it simplifies
458 the logical state preparation of the ancilla block.

459 The intuition is formalized through *covering map* between the topological structures (vertices, edges, and
460 faces) of the data and ancilla codes. Such a map induces corresponding linear mappings between their chain
461 complexes, ensuring that the homomorphic gadget conditions are automatically satisfied.

462 In this framework, the Steane measurement corresponds to a homeomorphic (one-to-one) chain map,
463 while the homomorphic logical measurement generalizes it to a *covering map* (locally bijective but globally
464 many-to-one). This broader formulation naturally supports more general and scalable constructions of logical
465 measurements across CSS codes.